

Chaos and stability in a two-parameter family of convex billiard tables

Péter Bálint¹, Miklós Halász¹, Jorge A. Hernández-Tahuilán²‡ and David P. Sanders²

¹ Institute of Mathematics, the Budapest University of Technology and Economics, Egrý József u. 1, H-1111, Budapest, Hungary

E-mail: `pet@math.bme.hu`, `miklos.halasz@yahoo.co.uk`

² Departamento de Física, Facultad de Ciencias, Universidad Nacional Autónoma de México, Ciudad Universitaria, 04510 México D.F., Mexico

E-mail: `dps@ciencias.unam.mx`

Abstract. We study, by numerical simulations and semi-rigorous arguments, a two-parameter family of convex, two-dimensional billiard tables, generalizing the one-parameter class of oval billiards of Benettin–Strelcyn [1]. We observe interesting dynamical phenomena when the billiard tables are continuously deformed from the integrable circular billiard to different versions of completely-chaotic stadia. In particular, we conjecture that a new class of ergodic billiard tables is obtained in certain regions of the two-dimensional parameter space, when the billiards are close to skewed stadia. We provide heuristic arguments supporting this conjecture, and give numerical confirmation using the powerful method of Lyapunov-weighted dynamics.

AMS classification scheme numbers: Primary: 37D50; Secondary: 37A25, 37J40, 37M25

1. Introduction

Billiard models are a class of Hamiltonian dynamical systems which exhibit the full range of behaviour from completely integrable to completely chaotic dynamics [2]. They consist of a point particle which collides elastically with the walls of a bounded region, the *billiard table*; the shape of the table determines the type of dynamics which is observed.

Several classes of two-dimensional billiard tables have been studied which interpolate between completely integrable and completely chaotic dynamics, including both one-parameter [1, 3, 4, 5, 6] and two-parameter [7] families. These allow us to observe the transitions by which the typical phase space, which is a mixture of ergodic, chaotic components, and regular KAM islands, evolves from one extreme behaviour to the other.

The chaotic limit is often represented by the Bunimovich stadium billiard, which consists of two semicircular arcs connected by two parallel line segments. When these two segments are non-parallel and one of the arcs is shorter, with the other being longer than a semicircle, we instead obtain the *skewed stadium* or *squash* billiard table. Such stadia are known to be ergodic and hyperbolic; however, as a consequence of so-called “quasi-integrable” phenomena, the hyperbolicity is non-uniform, and the dynamical behaviour is very sensitive to perturbations

‡ This paper is dedicated to the memory of Jorge Alejandro Hernández Tahuilán, who died tragically shortly after this paper was submitted. This work formed part of his Master’s thesis, and was to be his first published article.

37 of the boundary. There is an abundance of literature on stadium billiards; some works that are
38 relevant to our discussion are refs. [8, 9, 10, 11, 12]; see also section 2.1 for a more detailed
39 description of stadia.

40 In this paper, we study a two-parameter set of two-dimensional billiard tables which
41 generalizes the one-parameter family of oval billiards studied in refs. [1, 3] in a particular
42 way; see section 2.2 for an explicit description. Our models constitute a subcase of a rather
43 general class of billiards introduced, but not studied in detail, by Hayli and Dumont [13]. Our
44 class is of particular interest since it includes as limiting cases an entire family of ergodic
45 skewed stadium billiards. Here these are generalised by deforming the sides of the stadia to
46 circular arcs.

47 As in previous works on billiards formed from piecewise smooth components [1, 3, 13,
48 14, 7, 15, 16, 17, 18], for a large set of parameter values, we find coexistence of stability
49 islands and chaotic components in phase space. However, we also find numerically that
50 billiards which are sufficiently close to the limiting skewed stadia appear to have *no* remaining
51 stability islands – the phase space is completely filled by a single chaotic, ergodic component.
52 This motivates us to conjecture a new class of ergodic billiard tables. Similar conjectures have
53 been suggested for other billiard models of similar type – see, e.g., [7].

54 Our case is, however, different from previous studies in several respects. Firstly, the
55 new class introduced in this paper, and conjectured (for an open set of parameter values)
56 to be ergodic, consists of *convex* planar billiards. The issue of ergodicity versus KAM
57 islands in convex billiards has been the focus of continued interest for several decades. On
58 the one hand, Lazutkin’s fundamental theorem [19], and its strengthening by Douady [20],
59 show that a convex planar billiard with at least C^6 boundary cannot be ergodic, due to
60 the existence of caustics near the boundary of the billiard. Furthermore, recent results by
61 Bunimovich and Grigo [21, 22] show that elliptic islands arise in C^2 stadium-like billiards
62 (billiard tables constructed from stadia by replacing the discontinuity of the curvature with a
63 C^2 -smoothing).

64 On the other hand, several classes of convex planar billiards (with some discontinuity
65 points of the curvature) are proved to be ergodic (see section 2.1 for a partial list of
66 references). A common feature of these examples is the *defocusing* mechanism, which
67 requires that whenever a narrow beam of (initially) parallel rays completes a series of
68 consecutive reflections on one of the smooth focusing components of the billiard boundary, it
69 must pass through a conjugate point and become divergent before the next collision with the
70 curved (non-flat) part of the boundary; see [2, 21] for a more detailed description.

71 Defocusing (in this sense) cannot take place in our examples: since all boundary
72 components are curved, it would require that the discs which complete each circular arc
73 be contained inside the billiard table, which is prevented by the construction. Hence the
74 mechanism which produces the (conjectured) ergodic behaviour must be different. We are
75 aware of two other examples of ergodic planar billiards with focusing boundary components
76 where defocusing is violated [23, 24]; however, non-convexity of the billiard domain plays an
77 important role in both cases. Similarly, numerical studies in [7, 25] suggest ergodicity only
78 for certain *non-convex* domains.

79 Secondly, even though a rigorous proof is currently not available, we give, in addition
80 to the simulated phase portraits, further evidence which strongly supports our conjecture.
81 Heuristic arguments are provided in section 4, which rely on the similarity of the dynamics
82 with those of skewed stadia, and on the explicit analysis of sliding trajectories. The absence of
83 islands is then tested numerically by the powerful method of Lyapunov-weighted dynamics in
84 section 5. Before these arguments are given, the two-parameter family of generalised squashes
85 is defined in section 2, and some numerical results on the dependence of the dynamics on the

86 two geometrical parameters are presented in section 3.

87 2. The model

88 We begin by defining the class of generalised squash billiard models.

89 2.1. Convex billiard tables

90 Consider a convex, compact domain $Q \subset \mathbb{R}^2$ bounded by a closed, piecewise-smooth curve
 91 $\Gamma = \partial Q$. The motion of a point particle that travels along straight lines with constant speed
 92 in the interior of Q , and bounces off elastically (angle of reflection equals angle of incidence)
 93 when reaching the boundary Γ , is referred to as *billiard dynamics*.

94 We investigate these dynamics in discrete time, that is, from collision to collision. The
 95 phase space is then the cylinder $M = \Gamma \times [0, \pi]$, with $M \ni x = (k, \varphi)$, where the configurational
 96 coordinate is the arc length k along the boundary, which satisfies $0 \leq k < |\Gamma|$ and describes the
 97 point of the closed curve Γ at which the collision takes place, while the velocity coordinate
 98 $0 \leq \varphi \leq \pi$ describes the angle that the outgoing velocity makes with the (positively oriented)
 99 tangent line to Γ at the point k .

Given $x \in M$, the position and velocity at the next collision are uniquely determined, so
 that the billiard map $T : M \rightarrow M$ is well-defined (provided that the boundary of the table is C^1 -
 smooth). It is usual to visualize M as a rectangular domain in the plane, and the consecutive
 points along a trajectory of T as points in this domain. T has a natural invariant measure μ ,
 which is absolutely continuous with respect to Lebesgue measure on M , given by

$$d\mu = \text{const.} \sin \varphi \, dk \, d\varphi.$$

100 For further material on billiards in general we refer to the monographs [2, 26].

101 The billiard map may show a surprisingly wide variety of dynamical phenomena for
 102 different choices of the billiard table Γ . The best known case is the billiard in a circle: for this
 103 geometry the dynamics are *integrable*: the angle of incidence φ is an integral of motion, the
 104 values of which label the invariant curves [2].

105 If Γ is a $C^{5.5}$ -smooth closed curve, then for trajectories in the vicinity of the boundary
 106 the dynamics resemble, to some extent, those of the circular billiard: Lazutkin showed that a
 107 positive measure set of the phase space in a neighborhood of the boundaries $\varphi = 0$ and $\varphi = \pi$
 108 is foliated by invariant curves [19], and Douady later lowered the requirement to C^6 -smooth
 109 boundaries [20].

110 However, if Γ has less smoothness, then the billiard can be completely chaotic and
 111 ergodic. The first examples of such billiard tables are the celebrated stadia:

- 112 • the *straight stadium* is formed by two identical semicircles, joined at their endpoints by
 113 two parallel lines along their common tangents;
- 114 • the *skewed stadium*, or squash table, is formed by two circular arcs of different radii
 115 $r < R$, joined at their endpoints by non-parallel straight lines along their common
 116 tangents.

117 Stadia were introduced and their chaotic character first studied by Bunimovich in his
 118 famous paper [8]. It is known that for these tables the billiard map T is completely hyperbolic,
 119 i.e. there is one strictly positive and one strictly negative Lyapunov exponent for μ -a.e. $x \in M$,
 120 and T is ergodic with respect to μ ; see [10, 2, 27] for a detailed description of stadia.

121 Stadia have three important characteristic features:

- 122 • The table boundary Γ is only *piecewise* smooth: at the intersection points of the
123 circular arcs and straight lines, the curvature of the boundary (the second derivative)
124 is discontinuous. The resulting singularities play a crucial role in the dynamics of the
125 billiard map, both for the stadia and for the tables investigated below.
- 126 • The map T has many periodic points, all of which are either hyperbolic or parabolic. In
127 the case of the circular billiard, all periodic points are parabolic. We will see below that
128 in the generalised squash tables, the third class, elliptic periodic points, may also arise,
129 typically giving rise to KAM islands in their vicinity.
- 130 • The billiard map T in stadia is only *non-uniformly* hyperbolic. The reason for this is the
131 presence of so-called quasi-integrable – sliding, bouncing and diametrical – trajectory
132 segments of arbitrary length (see figure 8). When the geometry is perturbed, these quasi-
133 integrable phenomena may (or may not) create islands of integrability.

134 The mechanism that is responsible for the chaotic behaviour in stadium-shaped tables,
135 known as the *defocusing mechanism*, has also been observed and studied in other classes
136 of billiard tables in works of Bunimovich, Donnay, Markarian, Szász and Wojtkowski
137 [28, 29, 30, 31, 32, 33]. However, the geometry of the billiards studied in this paper is quite
138 different from the geometry of any of these classes.

139 2.2. The two-parameter family of generalised squashes

140 The family of convex billiard tables studied in this paper is described by two parameters, b and
141 c . The table is built on a trapezium, whose geometry is specified by the parameter $0 \leq b \leq 1$.
142 On each side of the trapezium is placed a circular arc joining its end-points, with adjacent arcs
143 constrained to meet with common tangents; the parameter $1 \leq c \leq \infty$ specifies the ratio of the
144 radii of the arcs.

145 More precisely, the base and the two sides of the trapezium are fixed to have unit length,
146 and b is the length of the top, which is parallel to the base. The two extreme cases $b = 0$ and
147 $b = 1$ correspond to the equilateral triangle and the square, respectively; see figure 1(a).

148 The table is left–right symmetric, with the circular arcs on the two sides having the same
149 radius. The radii of the arcs on the base, sides and top are denoted R , R_∞ and r , respectively.
150 As adjacent arcs are required to have a common tangent line where they meet, the shape of
151 the table is determined by the value of any one of the radii – for a given trapezium (value of
152 b), the geometry is parametrized by a single quantity, chosen for convenience to be the ratio
153 $c := R_\infty/R$; see figure 1. For brevity, throughout the paper the arcs corresponding to the base,
154 the sides and the top are referred to as the bottom arc, the “almost-flat” arcs, and the top arc,
155 respectively. The construction of the tables is detailed in the Appendix; they can be viewed as
156 a subfamily of a general class of billiards introduced in [13].

157 The case $c = 1$ gives a circle for any value of b ; the case $b = 1$ and $c = \infty$ corresponds to
158 the straight stadium; and the case $b < 1$ and $c = \infty$ gives a skewed stadium, with the amount
159 of skewness depending on the value of b . Thus, by changing c , we may continuously deform
160 the integrable dynamics of the circular billiard into a completely-chaotic billiard.

161 The transition for the case $b = 1$ (oval billiards based on a square) has previously been
162 studied [1, 3], although with a different parametrisation. In this paper, we concentrate instead
163 on the role of the parameter b , which determines the relative width of the top and bottom
164 sections of the billiard, and which leads to distinct phenomena for finite, but large enough,
165 c . We remark that an important role is played by so-called “quasi-integrable” phenomena,
166 which are common to all stadium-type billiards. These consist in arbitrarily long sequences
167 of collisions which do not contribute to hyperbolic behaviour; details are given in section 4.

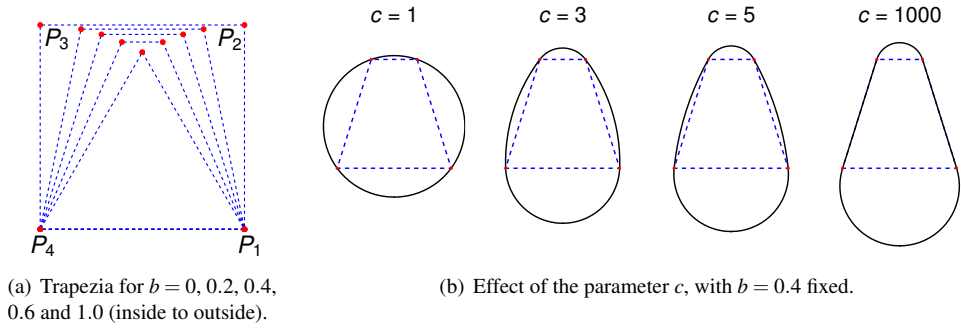


Figure 1. Variation of the geometry of the generalised squash billiards as a function of the two parameters b and c .

168 **3. Parameter-dependence of dynamics**

169 In this section, we survey the types of dynamical behaviour observed in numerical
 170 experiments in the two-dimensional (b, c) parameter space. The numerical methods used
 171 are briefly described in the Appendix. Numerical results for other billiard models formed by
 172 piecewise-smooth curves can be found in refs. [1, 3, 13, 14, 7, 15, 16, 17, 18].

173 *3.1. Parameter space*

174 It is useful to start from the known behaviour of the oval billiards obtained when $b = 1$
 175 [1, 3]. In this case, when $c = \infty$, the table is an ergodic straight stadium. As soon as c is
 176 decreased to a finite value, however, ergodicity of the billiard map is ruined. More precisely,
 177 *elliptic islands* – regions of positive Lebesgue measure which are foliated by invariant curves
 178 and concentrated around elliptic periodic points – appear in the phase space. For $c > 1$,
 179 coexistence of such elliptic islands and ergodic components of positive measure (“chaotic
 180 sea”) is observed. For large enough c , there is a single chaotic component (still coexisting
 181 with elliptic islands), while the number of chaotic components increases once c is decreased
 182 below certain thresholds. The references [1, 3] concentrate on this phenomenon of splitting
 183 of chaotic components.

184 The phenomenology is initially similar when we introduce $b < 1$. For c close to the
 185 limiting integrable case $c = 1$, the phase space is dominated by elliptic islands. For $c \gtrsim 1.2$
 186 it is already possible to observe a finite number of ergodic components, each of positive
 187 Lebesgue measure (“chaotic seas”) which fill most of the phase space, while for $c \gtrsim 1.5$ we
 188 observe a single, dominant ergodic component. The splitting of ergodic components studied
 189 in refs. [1, 3] occurs at $c \simeq 1.35$ when $b = 1$, while for $b < 1$ we observe similar phenomena,
 190 but restricted to a smaller range of c .

191 As we increase c further, the proportion of phase space occupied by elliptic islands has
 192 a tendency to decrease, and beyond a certain threshold, no remaining islands are numerically
 193 observed. This leads to our main conjecture (section 3.4) that the system is ergodic in a certain
 194 region of parameter space.

195 *3.2. Existence and stability regions of periodic orbits*

196 Elliptic islands are concentrated around elliptic periodic orbits, so studying the existence and
 197 stability properties of such orbits is critical [7]. For the $b = 1$ case, an important feature of

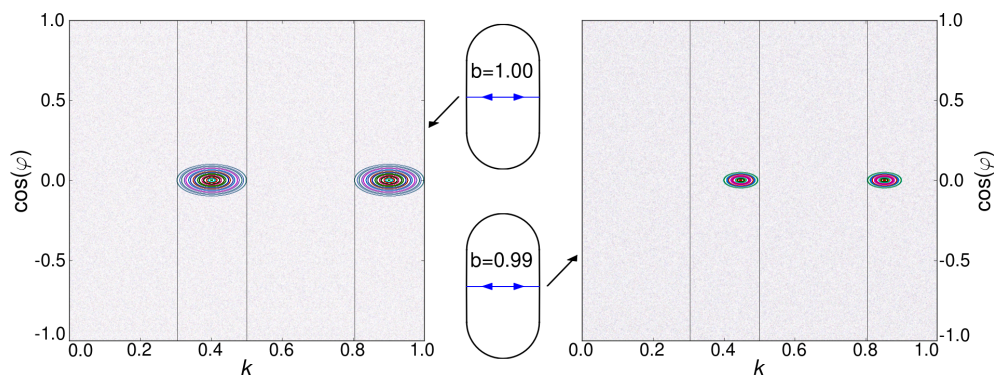


Figure 2. The period-2 orbit and corresponding island in phase space for $c = 100$ with $b = 1$ (left) and $b = 0.99$ (right).

the dynamics is a period-2 orbit which is present for *any* finite value of c , and which bounces perpendicularly between the midpoints of the almost-flat arcs. Its stability properties – in particular, the stability parameter s (cf. Appendix B) – can easily be calculated: when $c < \infty$ (that is, $R_\infty < \infty$), it is elliptic, and gives rise to an island. As shown in figure 2(a), the island around this orbit extends across the whole range of k along the almost-flat arcs, while its width in the φ direction decreases as c is increased.

For $b < 1$, however, the width of the island shrinks both in the k and in the φ directions as c is increased, as shown in figure 2(b), and finally *disappears* for large enough c . The reason is that the almost-flat arcs are now placed along two *non-parallel* sides of the trapezium, so that for large enough c there no longer exist points on these two arcs with mutually parallel tangent lines, and hence there is no such period-2 orbit. In this case, the bottom arc is forced to be longer than a semi-circle, due to the orientation of the tangent lines at the points where the bottom and almost-flat arcs join. The limit of existence of this period-2 orbit is thus when the bottom arc is exactly a semi-circle, which occurs at $c = c_0(b) := \frac{2}{1-b}$.

For $c > c_0(b)$, the period-2 orbit and its corresponding island disappear, but other islands, corresponding to periodic orbits of higher periods, appear in certain regions of the (b, c) plane. These islands generally appear in a certain window of values of c for a given, fixed b . Such stability regions for certain orbits of low period are shown in figure 3. For example, in the (blue) B region in the parameter space of figure 3, there exists an island around the period-4 orbit shown at the top right, for which the bounces on the bottom and left arcs are perpendicular (see also figure 4(a)).

3.3. Geometric destruction and period doubling of periodic orbits

A detailed study of the bifurcations occurring in the system is beyond the scope of this paper, and not our main goal here; instead, we give a short description of the main features that we have observed (see also [7]). We remark that bifurcation phenomena in piecewise-smooth systems are currently the subject of intensive studies – see e.g. [34, 35] and references therein.

Based on our observations, there are two kinds of dynamical phenomena that mainly determine whether an island of stability is formed around a periodic orbit. Firstly, the singularities of the boundary play an important role, since they influence the very existence of periodic orbits. To categorise such orbits, we use a coding of four symbols $\{B, R, T, L\}$, denoting bounces on the bottom, right, top and left arcs, respectively, and describe periodic

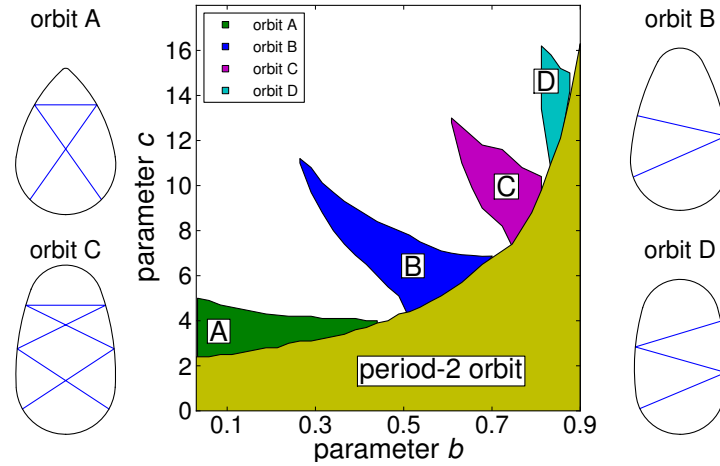
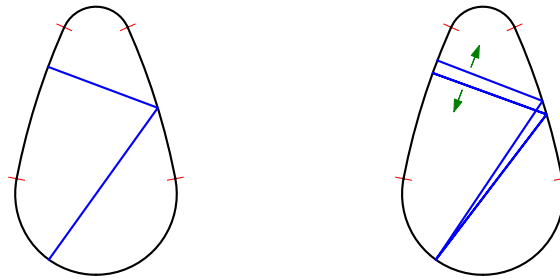


Figure 3. Regions of stability of certain types of periodic orbit. Each shaded region depicts the numerically-determined region of parameter space in which the corresponding labelled orbit type (with the same topology, or coding) is stable.

229 orbits according to a finite code (in general non-unique) of length equal to the orbit’s period.
 230 For example, consider again the period-2 orbit with code (R, L) , which consists of
 231 consecutive perpendicular bounces on the two almost-flat arcs, and which exists for $c < c_0(b)$.
 232 As c tends to $c_0(b)$ from below, the locations of the collision points on the sides move closer
 233 to the ends of the almost-flat arcs, finally reaching the lower corner points (singularities) when
 234 $c = c_0(b)$. For larger values of c , this period-2 orbit with code (R, L) ceases to exist, since
 235 there are no points on the almost-flat arcs with mutually parallel tangent lines. We refer to
 236 this as *geometric destruction* of the periodic orbit.
 237 However, geometric destruction is not the only mechanism by which an island
 238 corresponding to a periodic orbit may disappear. For example, figure 4(a) shows a period-
 239 4 orbit, around which an island of stability exists in the range $6.7 \lesssim c \lesssim 8.7$ for $b = 0.4$. When
 240 $c \simeq 8.7$, the orbit loses stability, even though its collision points are still located far from
 241 the singularities. In this case, the disappearance of the island is rather related to the stability
 242 properties of the periodic orbit.
 243 In the setting of *smooth* dynamical systems, it is known that when a periodic orbit
 244 loses stability (the stability parameter $|s|$ increases above 2, cf. Appendix B), *period-doubling*
 245 *bifurcations* may be observed; see eg. [36]. As observed in [7], this can also occur in billiards,
 246 provided the periodic orbit stays away from the singularities.
 247 Consider again the period-4 orbit studied above for $b = 0.4$. As c increases from $c \simeq 6.7$
 248 to $c \simeq 8.7$, the stability parameter s decreases from 2 to -2 ; see figure 6. When c reaches
 249 the critical value 8.7, the shape of the island changes and it splits into two components, the
 250 centers of which are consecutive points of a period-8 orbit, shown in figure 4(b). The changes
 251 in shape of the corresponding islands which surround the periodic orbits is shown in figure 5.
 252 The period-4 orbit indeed undergoes a period-doubling bifurcation, becoming hyperbolic and
 253 giving rise to an elliptic period-8 orbit, around which the island forms. As c is increased
 254 further, the geometry of the period-8 orbit is deformed, and soon a collision point reaches a
 255 corner, resulting in geometric destruction of the island.
 256 Similar period-doubling bifurcations occur for other periodic orbits when their
 257 disappearance is not due to geometric destruction. However, the presence of the singularities



(a) Period-4 orbit with $c = 8.59$. (b) Period-8 orbit with $c = 8.61$.

Figure 4. Period-doubling bifurcation of a period-4 orbit for $b = 0.4$ as c is varied. The (red) thin straight lines indicate the singularities in the boundary of the squash, where the circular arcs are joined. The arrows indicate the direction in which the trajectory moves as c increases.

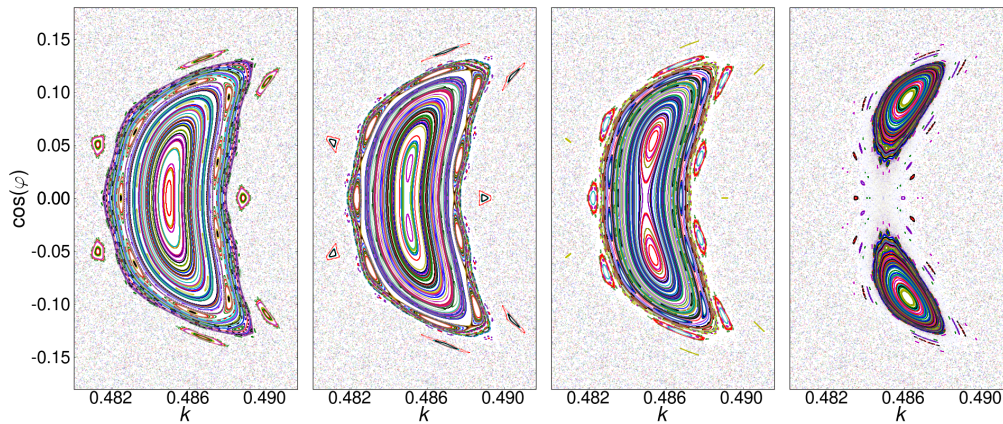


Figure 5. Phase-space structures for the period-doubling bifurcation of the elliptic periodic orbit shown in figure 4(a), highlighting the splitting of the corresponding island. Parameter values $b = 0.4$ and $c = 8.59, 8.61, 8.63$ and 8.69 from left to right.

258 modifies the picture significantly, so that islands are subject to the combination of two effects,
 259 geometric destruction caused by the singularities of the table, combined with the generic
 260 features characteristic of smooth systems with mixed phase space; see also [7, 37] for similar
 261 phenomena .

262 *3.4. Main conjecture: a class of ergodic convex billiards*

263 We now focus on the case of large c for some $b < 1$ fixed. The tendency is that as c increases,
 264 stability islands form around orbits of higher period. Typically, orbits of higher period are
 265 more sensitive to geometric destruction, since the presence of more bounces leads to more
 266 possibilities for one of the collision points to collide with a singularity when the parameters
 267 are varied. Thus the area in phase space of higher-period islands tends to decrease with
 268 increasing period. For this reason, the region in the parameter space where period-doubling

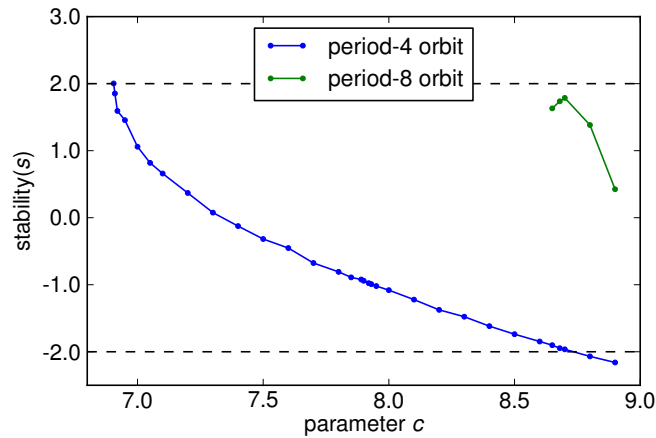


Figure 6. Dependence of the stability on c for the period-4 and period-8 orbits shown in figure 4.

269 bifurcation phenomena can actually be observed is quite limited.

270 Furthermore, as the parameter c is increased even further, it appears that *all* islands
 271 disappear, and that the system thus becomes ergodic. These numerical observations motivate
 272 the following conjecture:

273 **Main conjecture.** *For any $b < 1$, there exists $\hat{c}(b)$ such that for any pair of parameters (b, c)
 274 with $c > \hat{c}(b)$ the billiard dynamics are ergodic.*

275 That is, once the generalised squash billiards are close enough to skewed stadia, we
 276 conjecture that they are ergodic. There is an obvious lower bound $\hat{c}(b) \geq c_0(b)$ on the region
 277 of ergodicity in parameter space (cf. section 3.2); both quantities tend to ∞ as b tends to 1, i.e.
 278 in the limit of oval billiards, for which there is never ergodicity for $c < \infty$.

279 Similar conjectures have been made for certain regions of parameter space in other
 280 billiards with piecewise-smooth boundaries [7]. Here, however, we provide heuristic
 281 arguments, and confirmation using a more powerful numerical method, in the next two
 282 sections.

283 4. Heuristic support for the conjecture

284 In this section, we support our conjecture with heuristic arguments. Even though a rigorous
 285 proof, which appears to be a technically challenging task, is currently not available, we believe
 286 that we capture the key phenomena.

287 Our heuristic argument relies on a comparison of the dynamics of the model for large c
 288 with the limiting case $c = \infty$, i.e. the skewed stadia, which have been extensively studied. We
 289 first summarize the key characteristics of the dynamical behavior of these stadia ($c = \infty$); for
 290 more details, see in particular refs. [10, 11, 38].

291 4.1. Dynamics of skewed stadia ($c = \infty$)

292 On a large part of phase space, the billiard dynamics for stadia is strongly hyperbolic. It
 293 is, on the other hand, possible to locate precisely the places where hyperbolicity can be

294 arbitrarily weak: these correspond to quasi-integrable (bouncing, diametrical or sliding)
 295 trajectory segments, which can be analysed by direct geometrical arguments. Roughly, if one
 296 considers a smooth curve in the phase space that has completed a quasi-integrable segment of
 297 length $n_1 \gg 1$, then the points along this curve will begin another quasi-integrable segment
 298 of length $n_2 \gg 1$, and, assuming that the curve is sufficiently stretched out, it is possible to
 299 calculate the transition probabilities for the allowed $n_1 \rightarrow n_2$ transitions. By this analysis one
 300 observes that, on the average, n_2 is smaller than n_1 . This results in escaping from the quasi-
 301 integrable region: almost every point leaves this part of the phase space after a finite number
 302 of consecutive quasi-integrable segments.

303 The above behavior plays a crucial role in the analysis of stadia; it resulted, for example,
 304 in the proof of finer statistical properties like correlation decay rates and statistical limit laws
 305 [2, 10, 11] and in the investigation of survival probabilities [12]. As already mentioned above,
 306 a mathematically rigorous proof of our main conjecture is beyond the scope of the present
 307 paper. Instead, we argue that generalized squashes show a dynamical behavior very similar
 308 to the one sketched above. More precisely, on a large part of the phase space – in particular,
 309 apart from sliding trajectory segments – the dynamics for the $c = \infty$ and the finite $\bar{c} \gg 1$ cases
 310 are directly comparable. On the other hand, sliding trajectory segments can again be analysed
 311 by direct geometrical arguments, and we observe escape from the quasi-integrable region in
 312 the sense described above.

313 4.2. Notation and phase spaces

314 A key ingredient of our argument is the comparison of the billiard maps for $c = \infty$ and $\bar{c} \gg 1$,
 315 for the same value of $b < 1$. To compare the two maps, their phase spaces are identified by a
 316 map $\chi : M^{\bar{c}} \rightarrow M^\infty$, which is defined below. Throughout, upper indices refer to the value of c
 317 ($c = \infty$ or $\bar{c} \gg 1$ finite), which we omit if the description applies to both cases; later, we will
 318 also need to compare maps for different b , in which case the two upper indices (b, c) of the
 319 map will be given.

320 For $x = (k, \varphi) \in M$, with $0 \leq \varphi \leq \pi$ and $0 \leq k < |\Gamma|$, let $0 = k_0 < k_1 < k_2 < k_3 < k_4 = |\Gamma|$
 321 denote the arclength coordinates of the corner points separating consecutive arcs. We denote
 322 by M_B, M_R, M_T and M_L the sets of points (k, φ) with $k \in [k_0, k_1]$, $k \in [k_1, k_2]$, $k \in [k_2, k_3]$ and
 323 $k \in [k_3, k_4]$, respectively – that is, phase points on the bottom, right, top and left arcs. We also
 324 denote the angles of the bottom and top arcs by $2\alpha_B$ and $2\alpha_T$, respectively, so that $k_1 = 2R\alpha_B$
 325 and $k_3 - k_2 = 2r\alpha_T$, where R and r are the radii of the bottom and top arcs, respectively. The
 326 set $\bar{M} = \bar{M}_B \cup \bar{M}_T$, where

$$\bar{M}_B = \left\{ (k, \varphi) \in M_B \mid (\pi - \alpha_B) \frac{k}{k_1} \leq \varphi \leq (\pi - \alpha_B) \frac{k}{k_1} + \alpha_B \right\};$$

$$\bar{M}_T = \left\{ (k, \varphi) \in M_T \mid (\pi - \alpha_T) \frac{k - k_2}{k_3 - k_2} \leq \varphi \leq (\pi - \alpha_T) \frac{k - k_2}{k_3 - k_2} + \alpha_T \right\},$$

327 a union of two parallelograms, plays a special role in our discussion. Note that $x \in \bar{M}$ if
 328 and only if x is on the bottom arc and its image, Tx , is not on the bottom arc, and a similar
 329 characterization applies to \bar{M}_T with respect to the top arc. See Figure 7 for the geometry of
 330 these sets. As \bar{M} is of positive measure, the first return map $\bar{T} : \bar{M} \rightarrow \bar{M}$ is naturally defined,
 331 and for the case of $c = \infty$, $\bar{T}^\infty : \bar{M}^\infty \rightarrow \bar{M}^\infty$ is known to have strong hyperbolic properties – see
 332 eg. [10]. To exploit this fact, it is not so much the billiard maps $T^{\bar{c}}$ and T^∞ , but rather the first
 333 return maps \bar{T}^∞ and $\bar{T}^{\bar{c}}$, that we would like to compare.

334 This motivates the definition of the identification map $\chi : M^{\bar{c}} \rightarrow M^\infty$, as follows. Note
 335 that both $M_B \setminus \bar{M}_B$ and $M_T \setminus \bar{M}_T$ are unions of two triangles, hence the phase space M can

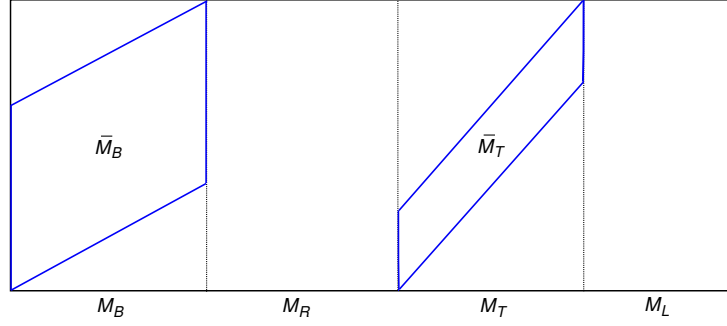


Figure 7. The sets \bar{M}_B and \bar{M}_T . The phase space is partitioned into 8 pieces on each of which the identification map χ is linear.

336 be regarded as a union of 8 polygonal pieces – two rectangles, two parallelograms and four
 337 triangles; see figure 7. The map $\chi : M^{\bar{c}} \rightarrow M^\infty$ is piecewise linear: it rescales linearly each
 338 of the 8 polygonal pieces of $M^{\bar{c}}$ onto the corresponding polygonal pieces of M^∞ . Note that χ
 339 matches the complete arcs of $M^{\bar{c}}$ with the complete arcs of M^∞ , and it matches $\bar{M}^{\bar{c}}$ with \bar{M}^∞ .
 340 Furthermore, the singularity set of χ and χ^{-1} is contained in the singularity set of $T^{\bar{c}}$ and T^∞ ,
 341 respectively. These properties ensure that \bar{T}^∞ and $\bar{T}^{\bar{c}}$ can be compared on a large part of \bar{M} ,
 342 specified precisely below. It is also worth noting that the identification map can be defined if
 343 the values of b are not equal in the cases $c = \bar{c}$ and $c = \infty$.

344 4.3. First-return maps

345 To proceed, we recall the notion of symbolic collision sequence (or code) from section 3.3:
 346 the symbolic sequence for the trajectory segment $(x, Tx, \dots, T^N x)$ is $A_N(x) = (a_0, a_1, \dots, a_N)$,
 347 where $a_i \in \{B, R, T, L\}$ specifies the arc (bottom, left, top or right) on which $T^i x$ is located.
 348 Note that the tangent map DT_x^N at $x \in M$ is well-defined if and only if $A_N(x)$ is unique, that
 349 is, none of the points $T^i x$ ($i = 0, \dots, N$) collides exactly at a corner (in other words, T^N is not
 350 singular at x). If x is singular, i.e. $T^i x$ lies at the corner point of two consecutive arcs for some
 351 $i \in \{0, \dots, N\}$, then a_i can take two possible values, hence several collision sequences, and,
 352 correspondingly, several tangent maps DT_x^N can be defined.

353 Now let us turn back to the investigation of the first-return map $\bar{T} : \bar{M} \rightarrow \bar{M}$. We recall
 354 an important property of the skewed stadium from [10]: \bar{T}^∞ is *uniformly hyperbolic*, in the
 355 following sense; there exists some $\Lambda > 1$ and cone fields C_x^s, C_x^u (stable and unstable cones) in
 356 the tangent bundle of \bar{M}^∞ , such that

- 357 (i) for $v \in C_x^u$, we have $D\bar{T}_x^\infty v \in C_{\bar{T}^\infty x}^u$ and $|D\bar{T}_x^\infty v| > \Lambda|v|$; and
 358 (ii) for $w \in C_{\bar{T}^\infty x}^s$, we have $(D\bar{T}_x^\infty)^{-1}w \in C_x^s$ and $|(D\bar{T}_x^\infty)^{-1}w| > \Lambda|w|$.

359 If \bar{T}^∞ is singular at x (i.e. the trajectory of $x \in \bar{M}^\infty$ hits at least one corner before returning to
 360 \bar{M}^∞), then properties (i) and (ii) above hold for the tangent map corresponding to any of its
 361 symbolic collision sequences.

362 Now, using the identification map χ , we argue that $\bar{T}^{\bar{c}}$ is also uniformly hyperbolic in the
 363 above sense, on a “large part” (specified below) of \bar{M}^∞ . First observe that the billiard tables for
 364 $c = \infty$ and $c = \bar{c}$ are piecewise C^2 -close – that is, the bottom, right, top and left arcs for $c = \bar{c}$
 365 are C^2 -close to their $c = \infty$ counterparts, as curves in the plane. We recall some properties
 366 of the billiard map from [2]; see also formula (B.1) in the Appendix. C^2 -closeness of the
 367 billiard tables would imply that the maps $T^{\bar{c}}$ and T^∞ are C^1 -close; however, the billiard map

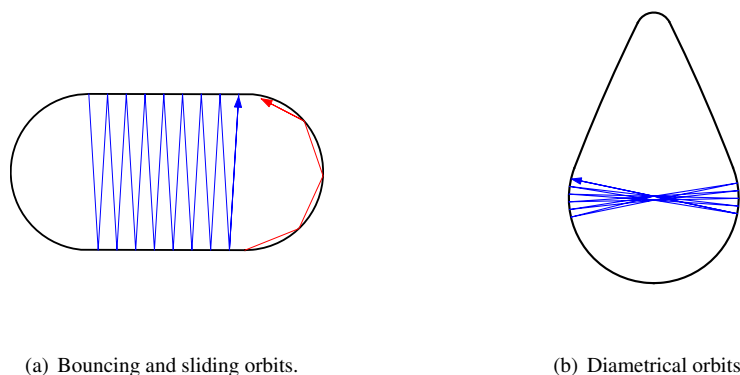


Figure 8. Quasi-integrable phenomena present in stadia.

368 is only piecewise smooth and may have unbounded derivatives corresponding to tangential
 369 collisions. Thus, $T^{\bar{c}}$ and T^∞ are C^1 -close unless $\varphi \simeq 0$ or $\varphi \simeq \pi$, in the following sense. For
 370 any $\varepsilon > 0$ there exists \bar{c} such that if $c > \bar{c}$, then given any $(k, \varphi) = x \in M_c$ with $\varepsilon < \varphi < \pi - \varepsilon$
 371 and symbolic collision sequence (a_0, a_1) , then there exists $x' \in M^\infty$ with the same collision
 372 sequence (a_0, a_1) , for which $d(x', \chi(x)) < \varepsilon$ and $d(T^\infty x', \chi(T^c x)) < \varepsilon$, and the tangent maps
 373 DT_x^c and $DT_{x'}^\infty$ are ε -close. If x is singular, then it is possible to find such $x' \in M^\infty$ for both of
 374 its collision sequences.

375 We would like to conclude that (apart from tangencies) $\bar{T}^{\bar{c}}$ is also C^1 -close to \bar{T}^∞ ,
 376 and thus, $\bar{T}^{\bar{c}}$ is also uniformly hyperbolic (as uniform hyperbolicity is a C^1 -open property).
 377 However, closeness of the T 's implies closeness of the \bar{T} 's only if phase points $x \in \bar{M}$ are
 378 considered for which $\bar{T}x = T^{n(x)}x$, such that $n(x)$, the number of iterates needed to return
 379 to \bar{M} , is *uniformly bounded*. Thus, we need to consider the complement of this set: points
 380 with unbounded return time, which are exactly the points from which the quasi-integrable
 381 trajectory segments originate. At this point the differences between the $b < 1$ and $b = 1$ cases
 382 play an important role, as follows.

383 4.4. Quasi-integrable phenomena

384 For *bouncing points* $x = (k, \varphi) \in \bar{M}$ (see figure 8(a)), returns to \bar{M} consist of a high number
 385 of consecutive collisions on the almost-flat arcs. If $b = 1$, then such orbits may spend an
 386 unbounded number of iterations bouncing close-to-perpendicularly on the almost-flat arcs.
 387 However, if $b < 1$, then the number of such bounces, and thus the time needed to return to \bar{M} ,
 388 is uniformly bounded (the bound, of course, depends on the actual value of b , which affects
 389 the value of $\hat{c}(b)$ in Conjecture 3.4).

390 *Diametrical quasi-integrable* motion, when the trajectory bounces back and forth
 391 between two diametrically-opposite points of a circle (figure 8(b)) may also correspond to
 392 unbounded return time. This phenomenon is dominated by the bottom arc of the $b < 1$ case:
 393 returns to \bar{M} consist of a diametrical trajectory segment (that can be arbitrarily long) and a
 394 single bounce on one of the almost-flat arcs. To see this, note that a long series of diametrical
 395 bounces is necessarily followed by a close-to-perpendicular bounce on one of the almost-flat
 396 arcs, close to the join of the boundary. Since the bottom arc is longer than a semicircle,
 397 the trajectory then returns immediately to the bottom arc almost parallel to a diameter, and

398 a new quasi-integrable segment begins. (See also [10] for a description of the dynamics of
 399 consecutive diametrical segments). As a consequence, the derivatives of the return maps \bar{T}^∞
 400 and $\bar{T}^{\bar{c}}$ can be directly compared at such points. In fact, here it is more useful to compare
 401 the maps $\bar{T}^{b,\bar{c}}$ and $\bar{T}^{\bar{b},\infty}$ with different values of the parameter b , where $\bar{b} \simeq b$ is chosen in
 402 such a way that the bottom arc of the skewed stadium for (\bar{b}, ∞) is identical to the bottom
 403 arc of the generalized squash for (b, \bar{c}) (the two arcs have equal radii and equal lengths) – the
 404 identification map $\chi : \bar{M}^{b,\bar{c}} \rightarrow \bar{M}^{\bar{b},\infty}$ can be easily generalized to this case. The advantage of
 405 this choice is that now it is possible to find $x' \in \bar{M}^{\bar{b},\infty}$ close to $\chi(x)$ such that the diametrical
 406 trajectory segments of x and x' are identical.

407 To compare the tangent maps for x and x' , we use the local orthogonal section (cf.
 408 Appendix B). Consider $x \in \bar{M}^{b,\bar{c}}$ with return time $n(x) = N + 1$ performing diametrical quasi-
 409 integrable motion, and let us denote the derivatives of the return maps by $D_N := D_x(\bar{T}^{\bar{b},\infty})$ and
 410 $\bar{D}_N := D_{x'}(\bar{T}^{b,\bar{c}})$. Let us introduce, furthermore, the matrix B_N , the tangent map corresponding
 411 to N consecutive diametrical bounces on the bottom arc (our choice of \bar{b} ensures that this part
 412 of the trajectory is identical in the two cases). Then $D_N = B_N \cdot A$ and $\bar{D}_N = B_N \cdot \bar{A}$, where the
 413 matrices A and \bar{A} are the tangent maps corresponding to the single bounce on the flat arc of the
 414 $c = \infty$ case and on the almost-flat arc of the $c = \bar{c}$ case, respectively. We have the following
 415 results:

- 416 • D_N is strongly hyperbolic, and expands unstable vectors at least by a factor $\kappa_1 \cdot N$ for
 417 some numerical constant $\kappa_1 > 0$ (see ref. [10]).
- 418 • All elements of the matrix B_N have absolute value less than $\kappa_2 \cdot N$ for some numerical
 419 constant $\kappa_2 > 0$ (this can be easily checked by direct computation based on Formula
 420 (B.1)).
- 421 • Choosing \bar{c} big enough, the difference of the matrices A and \bar{A} can be made arbitrarily
 422 small: that is, for any $\varepsilon > 0$, there exists some finite c' such that whenever $\bar{c} > c'$, we
 423 have $\|A - \bar{A}\| < \varepsilon$ (again from direct computation).

424 The above three facts imply that, choosing \bar{c} big enough, \bar{D}_N expands unstable vectors at
 425 least by a factor $\kappa_3 \cdot N$ for some positive constant κ_3 . In particular, at points that give rise to
 426 diametrical motion, uniform hyperbolicity of the return map persists for finite, big enough \bar{c} .

427 4.5. Analysis of sliding trajectories

428 For the third type of quasi-integrable motion, *sliding points* (figure 8(a)), the $c = \infty$ and the
 429 finite $c = \bar{c} \gg 1$ cases cease to be comparable, hence these points need to be analysed directly
 430 for finite c . Note also that sliding can occur only if $\varphi \simeq 0$ or $\varphi \simeq \pi$.

431 The above arguments can be summarized as follows: fix the parameters (b, c) where
 432 $b < 1$ and $c > \hat{c}(b)$. Then there exists $\varphi_{b,c}$ such that $\bar{T}^{b,\bar{c}}$ is uniformly hyperbolic for any
 433 $x \in \bar{M}^{b,\bar{c}}$ for which $\varphi_{b,c} < \varphi < \pi - \varphi_{b,c}$. Furthermore, for any fixed $b < 1$, $\varphi_{b,c} \rightarrow 0$ as $c \rightarrow \infty$.

434 In other words, the dynamics is strongly chaotic unless φ or $\pi - \varphi$ is very small, that
 435 is, unless the trajectory “slides along the boundary” of phase space (see eg. refs. [10] or
 436 [8] for this terminology). Below, we give a direct geometrical description of the dynamics
 437 within this sliding region. This is a delicate issue, as it is exactly in this part of phase space
 438 where Lazutkin constructed caustics, and, correspondingly, a positive-measure set foliated by
 439 invariant curves. The crucial difference here from Lazutkin’s setting is that the curvature of
 440 the boundary is discontinuous at the corner points which separate consecutive circular arcs.
 441 We will argue below that it is exactly these discontinuities that create “repulsion” from the
 442 sliding region.

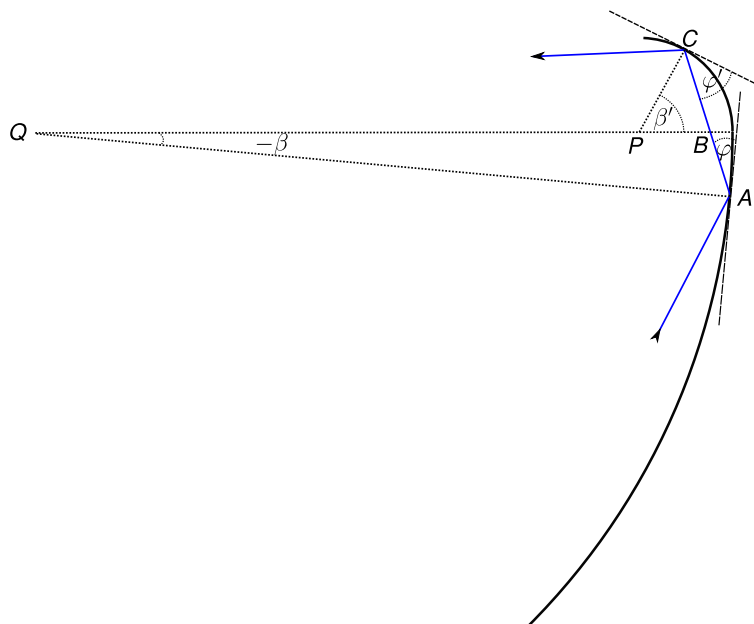


Figure 9. Geometry of switches between consecutive arcs.

443 In the rest of this section we fix $b < 1$ and $1 \ll c < \infty$, and omit upper indices. For
 444 concreteness, we describe the case when $\varphi \simeq 0$; the case when $\varphi \simeq \pi$ is completely analogous.
 445 In this region it is slightly more convenient to use, instead of the usual arclength k , the angular
 446 distance $\beta = k/R_{\text{arc}}$ along the arc of radius R_{arc} . Throughout, we will refer to the β coordinate
 447 as horizontal and the φ coordinate as vertical.

448 Since φ is small, the trajectory experiences a long series of consecutive collisions on the
 449 same circular arc. Provided this happens, evolution in the coordinates (β, φ) is given by

$$450 \quad (\beta', \varphi') := T(\beta, \varphi) := (\beta + 2\varphi, \varphi); \quad (1)$$

451 in particular, φ is an integral of motion. Then, after some time, the trajectory bypasses a corner
 452 point and switches to the neighboring arc, followed by another long series of consecutive
 453 bounces on that arc. Thus there is an alternation of long series of sliding along the same arc
 454 and “switches” from one arc to another. Below we argue that as an overall effect of switching
 455 transitions, the value of φ increases, which means that the trajectory escapes from the sliding
 456 region.

457 More precisely, instead of a single phase point, we investigate the evolution of a one-
 458 parameter family of phase points. We will say that a curve is *good* if in the (β, φ) coordinates
 459 it has either nonnegative slope, or its slope is negative but bounded away from the horizontal
 460 direction (it is enough to require that either $\frac{d\varphi}{d\beta} \geq 0$, or $\frac{d\varphi}{d\beta} \leq -\frac{1}{2}$). We consider a family of
 461 phase points smoothly distributed along a good curve, and show that the value of φ increases
 462 strongly on the average when this family evolves under the dynamics. Before investigating
 463 switches a little closer, let us remark that the twist map (1) tilts curves toward the horizontal
 464 direction. In particular, if a good curve (as defined above) is evolved by a high number of
 465 iterates of (1), then it is subject to horizontal stretching, and we get a curve of very small
 466 positive slope.

467 There are two types of transitions to be considered: switching from the bottom (or top)

468 arc to an almost-flat arc, an $R \rightarrow R_\infty$ transition, or from an almost-flat arc to the bottom (or top)
 469 arc, an $R_\infty \rightarrow R$ transition. We first consider an $R_\infty \rightarrow R$ transition, and denote the coordinates
 470 by (β, φ) just before the transition (last bounce on the bottom/top arc) and $(\beta', \varphi') = T(\beta, \varphi)$
 471 just after the transition (first bounce on the almost-flat arc). We normalize β such that $\beta = 0$
 472 corresponds to the corner point of the two arcs. Then $-2\varphi \leq \beta \leq 0$, and $0 \leq \beta' \leq 2\varphi'$ (see
 473 figure 9 for a sketch of the geometry). It is also convenient to introduce $\omega = \beta + \varphi$ and
 474 $\omega' = \beta' - \varphi'$. Note also that since the curve under consideration has experienced a long series
 475 of consecutive bounces on the almost-flat arc, its direction is close to horizontal, hence for
 476 fixed φ , ω may be regarded as evenly distributed on the interval $[-\varphi, \varphi]$. It is also apparent
 477 from figure 9 that the angles $\angle QBA$ and $\angle PBC$ sum up to π , hence $\omega' = \omega$. To express φ' in
 478 terms of φ and ω we use sine theorems for the triangles QAB and PBC on figure 9, giving

$$\begin{aligned} \frac{R_\infty - R + a}{R_\infty} &= \frac{|\overline{QB}|}{|\overline{QA}|} = \frac{\sin(\pi/2 - \varphi)}{\sin(\omega + \pi/2)} = \frac{\cos \varphi}{\cos \omega}, \\ \frac{a}{R} &= \frac{|\overline{PB}|}{|\overline{PC}|} = \frac{\sin(\pi/2 - \varphi')}{\sin(\pi/2 - \omega')} = \frac{\cos \varphi'}{\cos \omega}, \end{aligned}$$

479 where a denotes the length of the segment \overline{PB} , eliminating which we obtain

$$480 \quad c \cos \varphi = (c - 1) \cos \omega + \cos \varphi' \quad (\text{recall } c = R_\infty/R).$$

481 Approximating the cosines by second-order Taylor polynomials, we arrive at the following
 482 equations for $R_\infty \rightarrow R$ transitions:

$$483 \quad \omega' = \omega; \quad \varphi'^2 = c\varphi^2 - (c - 1)\omega^2. \quad (2)$$

484 Now let us take into account that $c \gg 1$. We have that, for fixed φ , φ' is essentially evenly
 485 distributed on the interval $[\varphi, \sqrt{c}\varphi]$, hence typically it is much larger than φ . To see this, let
 486 us apply the map (2) to the almost-horizontal curve that has completed a series of consecutive
 487 collisions on the almost-flat arc (for fixed φ , ω may be regarded as evenly distributed on the
 488 interval $[-\varphi, \varphi]$). Then the image is a curve in the (ω', φ') coordinates that is much more
 489 extended vertically than horizontally: it consists of a sharply-increasing part (connecting the
 490 points $(-\varphi, \varphi)$ and $(0, \sqrt{c}\varphi)$) and a sharply-decreasing part (connecting the points $(0, \sqrt{c}\varphi)$
 491 and (φ, φ)). For later reference, let us denote this curve by γ .

492 Note that the map (1) is expressed in terms of the (β, φ) coordinates, while the map (2)
 493 is expressed in terms of the (ω, φ) coordinates. Hence, before applying (2), the change of
 494 coordinates $(\beta, \varphi) \rightarrow (\omega, \varphi) = (\beta + \varphi, \varphi)$, and after applying (2), the change of coordinates
 495 $(\omega', \varphi') \rightarrow (\beta', \varphi') = (\omega' + \varphi', \varphi')$ are to be taken into account. However, as far as the
 496 geometry of curves is concerned, these coordinate changes can be regarded as additional
 497 applications of (1). In particular, it is enough to check that both parts of γ are good curves in
 498 the (ω', φ') coordinates. On the other hand, γ is far from being almost-horizontal. However,
 499 just after bypassing the corner point, the points of the curve start a long series of consecutive
 500 (sliding) bounces on the bottom (or top) arc. That is, the map (1) is applied many times, and
 501 as a result, the curve is strongly stretched along the horizontal direction. As a consequence, it
 502 can be partitioned into a large number of subcurves, the points of which reach the endpoint of
 503 the bottom arc simultaneously. Just before the $R \rightarrow R_\infty$ transition, all of these subcurves are
 504 almost horizontal.

505 We now turn to $R \rightarrow R_\infty$ transitions. Let us introduce the pre- and post-corner coordinates
 506 (ω, φ) and (ω', φ') , respectively. This time the quantities without primes correspond to the
 507 bottom (or top) arc, while the primed quantities correspond to the almost-flat arc. We obtain
 508 the same equations as above, with the role of φ and φ' interchanged:

$$509 \quad \omega' = \omega, \quad \varphi'^2 = \frac{1}{c}\varphi^2 + \left(1 - \frac{1}{c}\right)\omega^2. \quad (3)$$

510 Note that this time, for fixed φ , φ' is essentially evenly distributed on the interval $[\frac{1}{\sqrt{c}}\varphi, \varphi]$.
 511 Hence, even though φ' is smaller than φ , typically they are of the same order of magnitude.
 512 To see this, let us apply the map (3) to the curve that has just completed a long series of
 513 consecutive bounces on the bottom (or the top) arc; that is, for fixed φ , ω may be regarded
 514 as evenly distributed on the interval $[-\varphi, \varphi]$. The image is a curve in the (ω', φ') coordinates
 515 that has a decreasing and an increasing part: the former connects the points $(-\varphi, \varphi)$ and
 516 $(0, \frac{1}{\sqrt{c}}\varphi)$ with slope $\simeq -1$, while the latter connects the points $(0, \frac{1}{\sqrt{c}}\varphi)$ and (φ, φ) with
 517 slope $\simeq 1$; in particular, both parts are good curves. Now the points of this curve again
 518 start a series of consecutive bounces, this time on the almost-flat arc. By the time the next
 519 transition (this time an $R_\infty \rightarrow R$ transition) takes place, the curve has been subject to several
 520 applications of (1), which have stretched it in the horizontal direction, hence it consists of
 521 close-to-horizontal subcurves, the points of which bypass the corner point simultaneously.
 522 Then the whole argument can be iterated.

523 Let us make one more remark to avoid confusion. Of course, if we ran the dynamics
 524 backwards, we would need to apply the map (3) to the curve γ described above to obtain its
 525 *preimage* by an $R_\infty \rightarrow R$ transition. As (3) is the inverse of (2), we would obtain that the value
 526 of φ decreases by a factor $\frac{1}{\sqrt{c}}$ for most points of γ . However, γ is far from horizontal (actually,
 527 it is close to vertical) and the value of ω is far from being evenly distributed (actually, we have
 528 $|\omega| \ll \varphi$ for most points of γ). When investigating the forward dynamics, it is important that
 529 we apply both maps (3) and (2) to almost horizontal curves.

530 4.6. Summary

531 Summarising, for an overwhelming probability of phase points in our family (distributed
 532 smoothly along a good curve), the value of φ increases by a factor close to \sqrt{c} at $R_\infty \rightarrow R$
 533 transitions, and does not change drastically at $R \rightarrow R_\infty$ transitions. Overall, the value of φ
 534 thus increases on the average. Moreover, this increase is exponential in terms of the number
 535 of consecutive quasi-integrable (sliding) trajectory segments. Equivalently, we could say that
 536 the increase is exponential in terms of flow time, or in terms of the number of applications of
 537 the return map $\bar{T}^{\bar{c}}$. (Of course, the rate of increase in terms of the number of applications of
 538 the original map $T^{\bar{c}}$ can be arbitrary slow, as a single quasi-integrable segment may consist of
 539 an arbitrarily high number of bounces on the same arc).

540 Our argument above thus provides the following phenomenological description of the
 541 dynamics in generalised squashes with $b < 1$ and finite, but sufficiently large, c . The trajectory
 542 is subject to a strongly mixing dynamics in a large part of the phase space, away from the
 543 sliding region. From time to time, it makes excursions into the sliding region; however, on the
 544 average, it escapes from that region at an exponential speed. Note that these phenomena
 545 are completely analogous to what has been observed concerning consecutive bouncing
 546 trajectory segments in straight stadia, or consecutive diametrical segments of skewed stadia
 547 [10, 38, 11, 12]. Thus our observations provide strong support for our main conjecture.

548 These phenomena have been tested by convincing simulations, which can be reproduced
 549 by the reader using the program available at [39]. Note that on the phase portraits produced
 550 by this program, the configurational (horizontal) coordinate shown is k , rather than β , which
 551 should be kept in mind when comparing simulated trajectories with the above calculations.

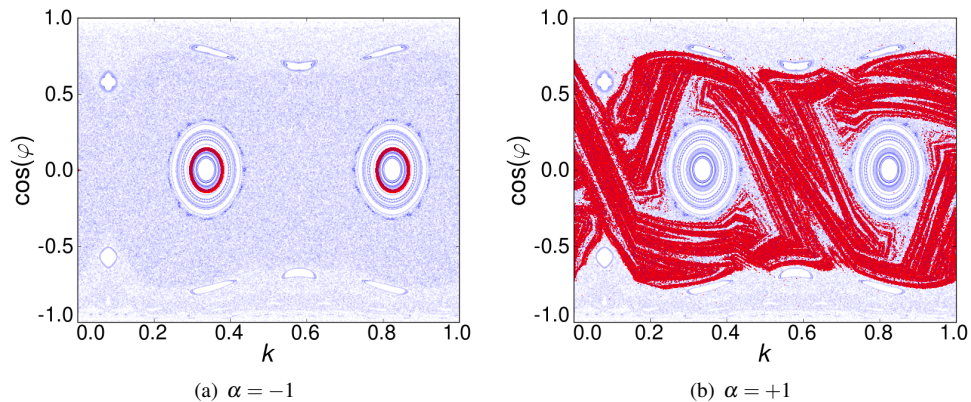


Figure 10. Results of applying LWD to a squash billiard with parameters $b = 0.6$ and $c = 1.6$, searching for both (a) regular and (b) chaotic regions. The thin (blue) points represent the evolution of randomly chosen initial conditions that evolve with the normal dynamics of the squash billiard, thus giving the standard representation of the phase space of the system. The (red) darker points show the superposition of the phase space locations during the last 100 collisions of 1000 walkers evolved under LWD for 10000 collisions.

552 5. Numerical evidence using Lyapunov-weighted dynamics

553 In this section, we look to support further our conjecture, by applying the powerful numerical
 554 method of Lyapunov-weighted dynamics to perform a more stringent search for elliptic
 555 islands in the two-dimensional (b, c) parameter space. The conjectured ergodic behaviour
 556 corresponds to the absence of such islands. Although no numerical method of this type can
 557 *prove* the absence of islands, we feel that the results presented here do provide support for the
 558 conjecture.

559 The simplest method to search for islands consists of sampling from a grid of initial
 560 conditions in phase space and estimating the Lyapunov exponent or an equivalent indicator
 561 [40] for each one. However, this is unreliable and time-consuming, since the number of initial
 562 conditions needed to locate an island is inversely proportional to the area of the island in phase
 563 space, and we are interested in small islands.

564 A more powerful approach to locate regions of phase space with regular (i.e. non-chaotic)
 565 dynamics is the *Lyapunov-weighted dynamics* method (LWD), introduced in ref. [41]. The
 566 idea of this method is to evolve a population of walkers under a modified version of the
 567 dynamics, chosen so that the cloud of walkers spontaneously *concentrates* in regions of phase
 568 space which have a large (respectively small) Lyapunov exponent, according to whether a
 569 parameter α of the method is positive (respectively negative) [41].

570 To do so, each walker follows the underlying deterministic dynamics of the system under
 571 study, but perturbed by a small random noise of strength ϵ . Each walker also carries a tangent
 572 vector, which evolves under the tangent dynamics of the map. The local stretching factor
 573 of this tangent vector is calculated, as in the standard calculation of Lyapunov exponents,
 574 and walkers are killed or copied (“cloned”) at a rate which is proportional to $(\alpha \text{ times})$ the
 575 stretching of their tangent vector [41]. This process can be shown to lead to the desired effect
 576 of the cloud of walkers “highlighting” the regions of chaotic or regular behaviour, depending
 577 on the value of α chosen [41]. Details of how the LWD method may be applied to billiard
 578 models will be discussed elsewhere.

579 Figure 10 illustrates the results of applying the LWD method to a generalised squash

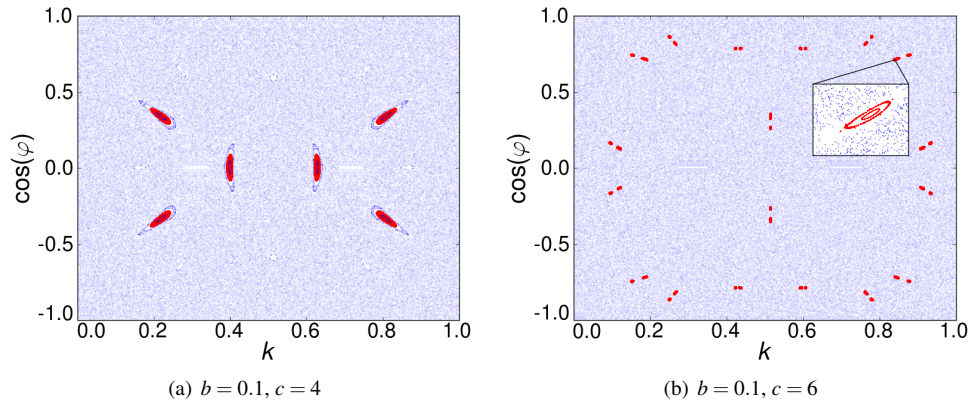


Figure 11. Results of applying LWD with $\alpha = -1$ to two squash billiards. The superposition of the last 100 collisions of 10000 walkers evolved under LWD for 10000 collisions is shown in (red) darker points on top of the phase space.

580 billiard, searching for both regular ($\alpha = -1$) and chaotic ($\alpha = +1$) dynamics. When $\alpha = -1$,
 581 the walkers concentrate in one of the elliptic islands of the phase space, whereas when $\alpha=1$,
 582 the walkers instead stay in part of a chaotic component of the phase space, as shown in figure
 583 10(b). In this case, there is in fact a partial barrier to transport in the phase space, visible
 584 around $\cos(\varphi) \simeq 0.7$ in figure 10. The LWD dynamics with $\alpha = +1$ nonetheless only sees
 585 part of this chaotic component.

586 Our approach is thus to exhaustively explore the (b, c) parameter space, looking for
 587 elliptic islands using LWD with $\alpha < 0$, in which case the walkers have a tendency to
 588 concentrate in the part of phase space which is “most stable”, and thus to highlight any elliptic
 589 islands present. To exemplify the findings, figure 11(a) shows the results of applying LWD
 590 to a squash billiard with parameters $b = 0.1$ and $c = 4$. For these parameter values, there is
 591 an elliptic periodic trajectory of period 6, around which there is an elliptic island, but there
 592 is also a set of parabolic periodic orbits, corresponding to diametrical bouncing, since the
 593 lower circular arc is longer than a semi-circle, as discussed in section 2.2. When LWD is
 594 applied, the walkers concentrate exclusively around the elliptic island, with none trapped near
 595 the parabolic orbits, as shown in figure 11(a). This preference for the more stable islands is
 596 independent of both the size and the period of the island, as indicated in figure 11(b), where
 597 there are two islands of period 18, as well as parabolic bouncing orbits, for $c = 6$.

598 If, however, we now increase c further, to $c = 13$, then all of the walkers concentrate
 599 around the *parabolic* orbits, as shown in figure 12(a). This strongly suggests that there are no
 600 longer any elliptic islands in phase space, which would be more stable, and that the system is
 601 thus ergodic.

602 Applying LWD with $\alpha > 0$, that is, searching for the chaotic region, instead shows a
 603 complicated fractal structure, as shown in figure 12(b). This corresponds to the region of
 604 phase space where the rate of expansion is maximised. This region appears to fill phase
 605 space in a non-uniform way, avoiding the parabolic orbits. For comparison, figure 13 shows
 606 the results of applying LWD to a known ergodic system, the Bunimovich stadium. Similar
 607 behaviour is found as for the squash billiard, reinforcing ergodicity for the squash.

608 Nonetheless, it is possible that for the squash billiard, tiny elliptic islands in phase space
 609 still remain, whose area is below the threshold which may be detected using the LWD method.
 610 This threshold is the consequence of the noisy nature of the method, which we intend to

611 explore in more detail elsewhere.

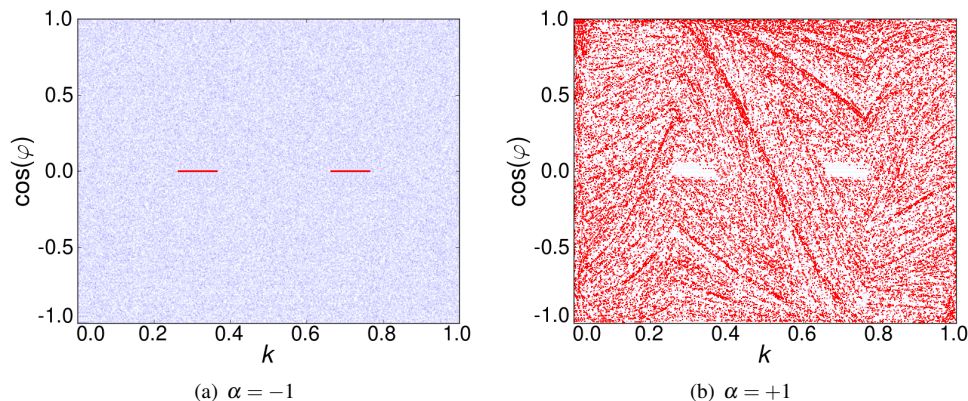


Figure 12. Results of applying LWD to a squash billiard with parameters $b = 0.1$ and $c = 13$. The superposition of the last 100 collisions of 1000 walkers evolved under LWD for 10000 collisions is shown in (red) darker points on top of the phase space.

612 Figure 14 shows the qualitative behaviour observed over the two-dimensional (b, c)
 613 parameter space for $c < 50$, i.e. whether or not any elliptic islands were found with LWD
 614 for each pair (b, c) . This picture provides strong evidence for our main conjecture, confirming
 615 that no islands are found by the method for c above a certain curve which is a function of
 616 b . The disappearance and reappearance of islands observed in the figure as c is increased for
 617 certain values of b is presumably related to the interplay of geometric destruction and complex
 618 series of period-doubling bifurcations [36] (see also section 3.3).

619 We have also sampled even larger values of c at random, observing the same behaviour
 620 shown in figure 12, where the walkers concentrate around the parabolic orbits. As far as the
 621 LWD method allows us to exclude the existence of elliptic islands, we thus obtain further
 622 evidence pointing towards our main conjecture that the system is ergodic for $c > \hat{c}(b)$.

623 6. Conclusions

624 We have studied the dynamics of a two-parameter class of generalised squash billiards, which
 625 interpolates between completely integrable and completely chaotic dynamics. We have shown
 626 that the dynamical properties in the two-dimensional parameter plane are rather rich, involving
 627 a mixture of period-doubling behaviour reminiscent of smooth dynamics, and destruction of
 628 orbits caused by collisions with corners of the billiard table.

629 We have conjectured, based on heuristic arguments which we hope can be made rigorous,
 630 and extensive numerical simulations with both standard and Lyapunov-weighted methods, that
 631 all elliptic periodic points and their associated islands disappear for tables which are close
 632 enough to skewed stadia, thus giving a previously unknown class of ergodic convex billiards.
 633 It remains to characterize the parameter space in more detail, and prove the conjecture.

634 Acknowledgements

635 We thank the anonymous referees for their valuable comments which resulted in a significant
 636 improvement of the paper. PB acknowledges useful discussions with S. Troubetzkoy back
 637 in 2004, where the idea of studying generalised squashes originated. He also acknowledges

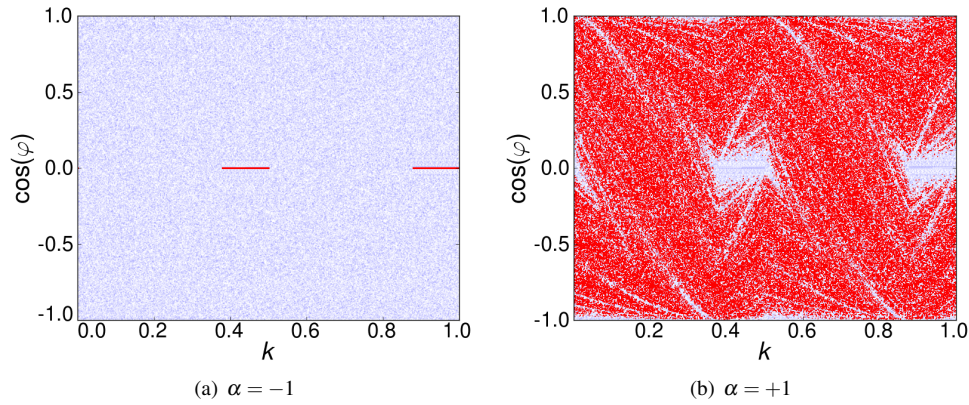


Figure 13. Results of applying LWD to an ergodic Bunimovich stadium. The superposition of the last 100 collisions of 1000 walkers evolved under LWD for 10000 collisions is shown in (red) darker points on top of the phase space.

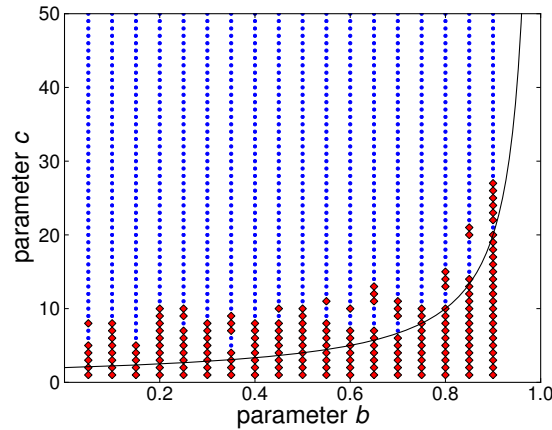


Figure 14. Parameter space of the generalised squash billiard. LWD with 1000 walkers evolving during 2000 collisions is applied to find regular regions ($\alpha = -1$). Pairs (b, c) that have elliptic islands found in this way are shown with (red) diamonds; pairs that do not have them are shown with (blue) points. The black continuous curve corresponds to $c_0(b)$.

638 financial support from the Bolyai Scholarship of the Hungarian Academy of Sciences, and
 639 OTKA (Hungarian National Fund for Scientific Research) grants F60206 and K71693. DPS
 640 acknowledges useful discussions with T. Gilbert and B. Krauskopf, and financial support from
 641 DGAPA-UNAM PAPIIT grant IN105209 and CONACYT grant CB101246.

642 **Appendix A. Construction of generalised squash billiards**

643 In this appendix, we sketch the geometric construction of generalised squash billiards. For
 644 fixed values of the parameters b and c , we must determine the radii and centers of the circular
 645 arcs that make up the table so that they satisfy the conditions of having common tangents at
 646 their points of intersection. To determine these quantities, we use the notation of Figure A1.

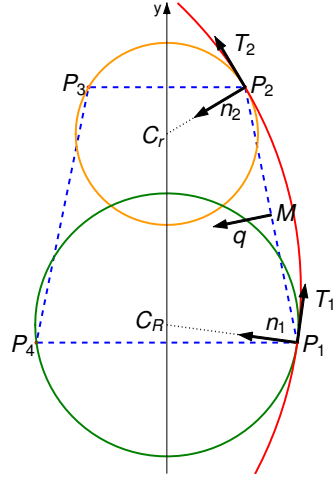


Figure A1. Geometry of generalised squash billiards. The trapezium is shown in (blue) dashed lines for a generic value of b . The different circular arcs are shown in different grey scales (colours).

647 Fixing the parameter b determines the length of the top of the trapezium and the points
 648 P_1, P_2, P_3 and P_4 . Since the table is symmetric about the vertical axis, it is only necessary to
 649 satisfy the tangent conditions for three arcs, since the right and left arcs have the same radii
 650 and their centers are reflected in the vertical axis.

651 The upper circular arc has radius r and center C_r , the lower arc has radius R and center
 652 C_R , and the right arc has radius R_∞ and center C_{R_∞} . Denote by M the midpoint of the segment
 653 joining P_1 and P_2 , and by q a vector perpendicular to this segment.

654 By symmetry, C_r is on the y -axis, taking a suitable Cartesian coordinate system. Since
 655 $\|P_2 - C_r\| = r$, we have

$$656 \quad C_r = \left(0, P_{2y} - \sqrt{r^2 - P_{2x}^2} \right). \quad (\text{A.1})$$

657 This allows us to calculate the tangent to the upper circular arc T_2 at P_2 , obtaining $T_2 =$
 658 $(C_r - P_2)_\perp$, where v_\perp denotes a vector perpendicular to a given vector v .

659 Let us denote, furthermore, by n_2 the unit vector perpendicular to T_2 . Since $C_{R_\infty} =$
 660 $P_2 + sn_2$, with $s \in \mathbb{R}$, we have $T_2 \cdot C_{R_\infty} = T_2 \cdot P_2$. Moreover, since C_{R_∞} is on the line through M
 661 with direction q , we find

$$662 \quad C_{R_\infty} = M + t_2 q, \quad \text{where } t_2 = \frac{T_2 \cdot P_2 - T_2 \cdot M}{T_2 \cdot q}. \quad (\text{A.2})$$

663 With this we can calculate the tangent to the lower arc at the point P_1 , obtaining
 664 $T_1 = (C_{R_\infty} - P_1)_\perp$.

665 Finally, $T_1 \cdot C_R = T_1 \cdot P_1$ and C_R is on the vertical axis, so

$$666 \quad C_R = (0, t_1), \quad \text{where } t_1 = \frac{T_1 \cdot P_1}{T_{1y}}. \quad (\text{A.3})$$

667 These equations give us C_R and C_{R_∞} as a function of r , since T_2 is a function of r and T_1
 668 is function of C_{R_∞} , which is also a function of r . Substituting these equations in the definition
 669 of the parameter c , we obtain

$$670 \quad c = \frac{R_\infty}{R} = \frac{\|C_{R_\infty} - P_1\|}{\|C_R - P_2\|}, \quad (\text{A.4})$$

671 giving an implicit equation for r in terms of b and c :

$$672 \quad 0 = f(r, b, c) = \|C_{R_\infty} - P_1\| - c\|C_R - P_2\|. \quad (\text{A.5})$$

673 This equation may be solved numerically, for example by bisection, to find the value of r
674 corresponding to given values of b and c . This can then be substituted back into equations
675 (A.2) and (A.3) to get C_{R_∞} and C_R , and with this we obtain the radii of the other arcs:

$$676 \quad R_\infty = \|C_{R_\infty} - P_1\|; \quad (\text{A.6})$$

$$677 \quad R = \|C_R - P_2\|. \quad (\text{A.7})$$

678 Appendix B. Numerical methods

679 The dynamics of generalised squashes may be simulated by standard methods, namely
680 finding the intersection of the particle trajectory with the circular arcs forming the boundary.
681 Periodic orbits may then be found by searching for iterates whose coordinates lie in a small
682 neighborhood of a given initial condition.

683 The stability properties of a periodic orbit may be calculated using the tangent map of the
684 dynamics, for which it is useful to take the (outgoing) local orthogonal section of the billiard
685 map [2], rather than phase space coordinates. Coordinates just after collision are taken as
686 the position $r \in Q$ and the velocity $v \in \mathbb{S}^1$; perturbations, up to linear order, are given by the
687 coordinates (dr, dv) , with both dr and dv perpendicular to the velocity v . Fix a phase point
688 $x = (k, \varphi) \in M$, and denote its image under the dynamics as $x' = Tx = (k', \varphi') \in M$. Denote
689 by K' the curvature of Γ at k' , and by τ the free path (distance between k and k'). Then the
690 image of a tangent vector (dr, dv) at x is the tangent vector (dr', dv') at x' , given by [2]

$$691 \quad \begin{pmatrix} dr' \\ dv' \end{pmatrix} = D \begin{pmatrix} dr \\ dv \end{pmatrix} = \begin{pmatrix} 1 & \tau \\ \frac{2K'}{\sin \varphi'} & 1 + \frac{2K'\tau}{\sin \varphi'} \end{pmatrix} \begin{pmatrix} dr \\ dv \end{pmatrix}. \quad (\text{B.1})$$

692 The tangent map for a higher iterate may be calculated as the product of several such
693 matrices. In particular if x is a periodic point of period p , i.e. $T^p x = x$, then it is possible to
694 consider $D_p = D_x(T^p)$. In the local orthogonal section coordinates, the billiard map is area
695 preserving, i.e. it has determinant 1. Thus the eigenvalue spectrum of D_p is characterized by
696 the trace s of D_p : the orbit is hyperbolic, parabolic or elliptic, according as $|s| > 2$, $|s| = 2$ or
697 $|s| < 2$, respectively. Hence s may be regarded as the *stability parameter* of the periodic orbit.
698 Similarly, Lyapunov exponents of orbits may be estimated as the exponential growth rate with
699 n of the trace of the product matrix giving the tangent map of the n th iterate.

700 References

- 701 [1] G. Benettin and J. M. Strelcyn. Numerical experiments on the free motion of a point mass moving in a plane
702 convex region: Stochastic transition and entropy. *Phys. Rev. A*, 17:773–785, 1978.
- 703 [2] N. Chernov and R. Markarian. *Chaotic Billiards*. Amer. Math. Soc., 2006.
- 704 [3] M. Hénon and J. Wisdom. The Benettin–Strelcyn oval billiard revisited. *Physica D*, 8(2), 1983.
- 705 [4] L.A. Bunimovich. Mushrooms and other billiards with divided phase space. *Chaos*, 11, 2001.
- 706 [5] R. Markarian, S. Oliffson Khamporst, and S. Pinto de Carvalho. Chaotic properties of the elliptical stadium.
707 *Comm. Math. Physics*, 174:661–679, 1996.
- 708 [6] C. Foltin. Billiards with positive topological entropy. *Nonlinearity*, 15:2053–2076, 2002.
- 709 [7] Holger R. Dullin, Peter H. Richter, and Andreas Wittek. A two-parameter study of the extent of chaos in a
710 billiard system. *Chaos*, 6(1):43, 1996.
- 711 [8] L.A. Bunimovich. On ergodic properties of certain billiards. *Func. Anal. Appl.*, 8(3):254–255, 1974.
- 712 [9] Roberto Markarian. A lower bound for chaos on the elliptical stadium. *Physica D*, 115(4):189–202, 1998.
- 713 [10] N. Chernov and H.-K. Zhang. Billiards with polynomial mixing rates. *Nonlinearity*, 18:1527–1553, 2005.

- 714 [11] Péter Bálint and Sébastien Gouëzel. Limit theorems in the stadium billiard. *Comm. Math. Phys.*, 263(2):461–
715 512, 2006.
- 716 [12] C. P. Dettmann and O. Georgiou. Survival probability for the stadium billiard. *Physica D*, 238:2395–2403,
717 2009.
- 718 [13] A. Hayli and Th. Dumont. Expériences numériques sur des billards C1 formés de quatre arcs de cercles. *Cel.
719 Mech. Dyn. Astr.*, 38(1):23–66, 1986.
- 720 [14] Avram Hayli. Numerical exploration of a family of strictly convex billiards with boundary of class c^2 . *J. Stat.
721 Phys.*, 83:71–79, 1996. 10.1007/BF02183640.
- 722 [15] V Lopac, I Mrkonjic, and D Radic. Chaotic behavior in lemon-shaped billiards with elliptical and hyperbolic
723 boundary arcs. *Phys. Rev. E*, 64, 2001.
- 724 [16] V Lopac, I Mrkonjic, and D Radic. Chaotic dynamics and orbit stability in the parabolic oval billiard. *Phys.
725 Rev. E*, 66, 2002.
- 726 [17] V. Lopac, I. Mrkonjic, N. Pavin, and D. Radic. Chaotic dynamics of the elliptical stadium billiard in the full
727 parameter space. *Physica D*, 217:88–101, 2006.
- 728 [18] V. Lopac and A. Simic. Chaotic properties of the truncated elliptical billiards. *Comm. Nonlin. Science Numer.
729 Simul.*, pages –, 2010. In press.
- 730 [19] V. F. Lazutkin. On the existence of caustics for the billiard ball problem in a convex domain. *Math. USSR Izv.*,
731 pages 185–215, 1973.
- 732 [20] R. Douady. *Applications du théorème des tores invariants. Thèse de 3ème cycle*. PhD thesis, Université Paris
733 VII, 1982.
- 734 [21] A. Grigo. *Billiards and Statistical Mechanics*. PhD thesis, Georgia Institute of Technology, 2009.
- 735 [22] L. Bunimovich and A. Grigo. Focusing components in typical chaotic billiards should be absolutely focusing.
736 *Comm. Math. Physics*, 293(1):127–143, 2010.
- 737 [23] L. Bussolari and M. Lenci. Hyperbolic billiards with nearly flat focusing boundaries, i. *Physica D*,
738 237(18):2272–2281, 2008.
- 739 [24] L. Bunimovich and G. del Magno. Track billiards. *Comm. Math. Physics*, 288(2):699–713, 2009.
- 740 [25] Holger R. Dullin and Arnd Bäcker. About ergodicity in the family of limaçon billiards. *Nonlinearity*,
741 14(6):1673, 2001.
- 742 [26] Serge Tabachnikov. *Billiards*. Société Mathématique de France, 1995.
- 743 [27] N. Chernov and H. K. Zhang. Regularity of Bunimovich’s stadia. *Reg. Chaotic Dyn.*, 12:335–356, 2007.
- 744 [28] M. Wojtkowski. Principles for the design of billiards with nonvanishing Lyapunov exponents. *Comm. Math.
745 Physics*, 105:391–414, 1986.
- 746 [29] R. Markarian. Billiards with Pesin region of measure one. *Comm. Math. Physics*, 118:87–97, 1988.
- 747 [30] V. Donnay. Using integrability to produce chaos: billiards with positive entropy. *Comm. Math. Physics*,
748 141:225–257, 1991.
- 749 [31] L. A. Bunimovich. On absolutely focusing mirrors. In U. Krengel et al., editor, *Ergodic Theory and related
750 topics, III*, number 1514 in Lecture Notes in Mathematics, pages 62–82. Springer-Verlag, 1992.
- 751 [32] D. Szász. On the K -property of some planar hyperbolic billiards. *Comm. Math. Physics*, 145:595–604, 1992.
- 752 [33] R. Markarian. New ergodic billiards: exact results. *Nonlinearity*, pages 819–841, 1993.
- 753 [34] M. Di Bernardo, C.J. Budd, A.R. Champneys, and P. Kowalczyk. *Piecewise-Smooth Dynamical Systems:
754 Theory and Applications*, volume 163 of *Applied Mathematical Sciences*. Springer Verlag, 2008.
- 755 [35] D.J.W. Simpson and J.D. Meiss. Simultaneous border-collision and period-doubling bifurcations. *Chaos*,
756 19:033146, 2009.
- 757 [36] R. S. MacKay. *Renormalisation in Area-Preserving Maps*, volume 6 of *Advanced Series in Nonlinear Dynamics*.
758 World Scientific, 1993.
- 759 [37] A. Arroyo, R. Markarian, and D. P. Sanders. Bifurcations of periodic and chaotic attractors in pinball billiards
760 with focusing boundaries. *Nonlinearity*, 22(7):1499–1522, 2009.
- 761 [38] N. Chernov and H.-K. Zhang. Improved estimates for correlations in billiards. *Comm. Math. Phys.*,
762 277(2):305–321, 2008.
- 763 [39] Miklós Halász. Computer software freely available at [http://www.renyi.hu/~bp/miki/program/
764 readme.html](http://www.renyi.hu/~bp/miki/program/readme.html).
- 765 [40] Zs. Sándor, B. Érdi, A. Széll, and B. Funk. The relative Lyapunov indicator: an efficient method of chaos
766 detection. *Celest. Mech. Dyn. Astron.*, 90(2):127–138, 2004.
- 767 [41] J. Tailleur and J. Kurchan. Probing rare physical trajectories with Lyapunov Weighted Dynamics. *Nature
768 Phys.*, 3:203–207, 2007. See also the Supplementary Information.